ACS OMEGA

Open Access

http://pubs.acs.org/journal/acsodf

Article

Antibacterial Efficacy of ZnO/Bentonite (Clay) Nanocomposites against Multidrug-Resistant *Escherichia coli*

Susanta Kumar Behera, Gausal A. Khan,* Swati Sucharita Singh, Bhumika Jena, Kali Sashank, Srinivas Patnaik, Ramesh Kumar, Byong-Hun Jeon,* Sankha Chakrabortty, Suraj K. Tripathy, and Amrita Mishra*

Cite This: *ACS Omega* 2024, 9, 2783−2794

Read Online

ACCESS | Metrics & More | Article Recommendations

ABSTRACT: The emergence of multidrug-resistant (MDR) bacteria has spurred the exploration of therapeutic nanomaterials such as ZnO nanoparticles. However, the inherent nonspecific toxicity of ZnO has posed a significant obstacle to their clinical utilization. In this research, we propose a novel approach to improve the selectivity of the toxicity of ZnO nanoparticles by impregnating them onto a less toxic clay mineral, Bentonite, resulting in ZB nanocomposites (ZB NCs). We hypothesize that these ZB NCs not only reduce toxicity toward both normal and carcinogenic cell lines but also retain the antibacterial properties of pure ZnO nanoparticles. To test this hypothesis, we synthesized ZB NCs by using a precipitation technique and confirmed their structural characteristics through X-ray diffraction and Raman spectroscopy. Electron microscopy revealed composite particles in the size range of 20−50 nm. The BET surface area of ZB NCs, within a relative pressure (P/P_0) range of 0.407−0.985, was estimated to be 31.182 m^2/g. Notably, 50 mg/mL ZB NCs demonstrated biocompatibility with HCT 116 and HEK 293 cell lines, supported by flow cytometry and fluorescence microscopy analysis. In vitro experiments further confirmed a remarkable five-log reduction in the population of MDR *Escherichia coli* in the presence of 50 mg/mL of ZB NCs. Antibacterial activity of the nanocomposites was also validated in the HEK293 and HCT 116 cell lines. These findings substantiate our hypothesis and underscore the effectiveness of ZB NCs against MDR *E. coli* while minimizing nonspecific toxicity toward healthy cells.

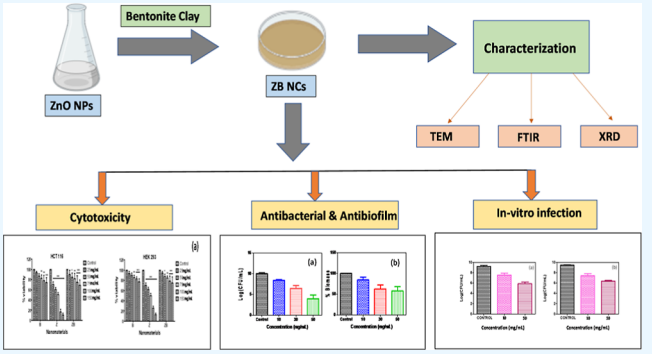

1. INTRODUCTION

The designing, processing, and application of materials in the nanoscale regime has remarkably advanced our gambit against scientific, technological, and social challenges and continues to endure an ever increasing interest.[1,2] Among various nanomaterials, zinc oxide nanoparticles (ZnO NPs), owing to their unique surface chemistry, quantum size dependent properties, and tailorable morphology, have been one of the most widely, scientifically explored, and industrially exploited material.[3,4] ZnO NPs are reported to have unique and remarkable applications in and/or as photocatalysts, optoelectronics, electrical devices, renewable energy devices, etc.[5−7] Moreover, a recent surge of reports and patents regarding the antibacterial potential of the ZnO materials has received ambivalent response from various stake holders.[8−10] The increase in bacterial infection and increasing resistance toward conventional antibiotics can affect public health and cause serious problem. So far, several mechanisms of antibiotic resistance have been discovered which includes the acquisition of transposons or plasmids coding for resistance genes, the upregulation of multidrug efflux pumps that pump out antibiotics, the inactivation of antibiotics by particular enzymes, the sequestration of antibiotics, the thickening of the cell wall preventing antibiotic entry, and the mutation of genes coding for antibiotic target proteins.[11,12] Finding innovative treatments to combat multidrug-resistant (MDR) microorganisms, particularly bacteria, is a crucial concern.[13] Such concerns have further intensified investigation of nanosized ZnO for real life applications.[14] Among various bacteria, *Escherichia coli* although a common flora of human gut, is infamous for causing many common bacterial infections, including cholecystitis, bacteremia, cholangitis, urinary tract infection, traveler's diarrhea, and other clinical complications

Received: October 11, 2023
Revised: December 15, 2023
Accepted: December 21, 2023
Published: January 5, 2024

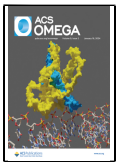

such as neonatal meningitis and pneumonia.[15] The development of MDR variants of *E. coli* has received the attention of scientists and clinicians due to their ability to resist many of the clinically used antibiotics and hence pose a serious challenge to global public health.[15−17] Therefore, in the recent past unconventional materials having antibiotic potential (e.g., ZnO nanostructures) have been particularly scrutinized as alternative candidates to counter the threat of the newly evolved MDR strains. Zhang et al. has reported the antibacterial activity of ZnO NPs against *E. coli*.[18] Kumar et al. suggested that ZnO NPs induce oxidative stress and DNA damage which leads to the reduced viability of *E. coli*.[19] Jiang et al. showed that both physical and chemical interactions contributed to the antibacterial behavior of ZnO NPs against *E. coli*.[20] Baek et al. reported the reactive oxidative stress-mediated antibacterial activity of engineered ZnO NPs against *E. coli*.[21] Antibacterial activity of pure and doped ZnO NPs against extended-spectrum beta-lactamases producing antibiotic-resistant *E. coli* was investigated by Hameed et al.[22] These inspiring research, however, could not propel the clinical trial and therapeutic applications because of following shortcomings: (1) indiscriminate toxicity of ZnO NPs toward targeted bacteria and nonspecific cells and tissues and (2) agglomeration of ZnO NPs with respect to time which may seriously diminish its antibacterial potential.[23,24] Recently, efforts have been made to synthesize tailor-made ZnO-based nanocomposites (NCs) to ameliorate the biocompatibility and stability of the resultant system. Khan et al. reported the enhanced biocompatibility of ZnO NPs by conjugation with Au and Ag NPs.[25,26] Rao et al. reported the synthesis of biocompatible carboxymethyl chitosan-ZnO NCs.[27] Similarly, Zhu and co-workers studied the enhanced biocompatibility of polyacrylate/ZnO NCs.[28] Although these systems could downregulate the toxicity of the ZnO NPs toward the studied cells, requirement of sophisticated synthetic protocols, arguable stability under harsh conditions, and inordinate costing crippled their therapeutic applications. Lately, clay matrixes have offered an inveigle opportunity considering their large scale availability, stability under harsh conditions, well studied biocompatibility as well as proven medicinal and cosmetic significance.[29] Additionally, clay minerals for a long time are studied for their intrinsic antibacterial properties.[30] Tokarský et al. reported the reduction of phytotoxicity of ZnO/Kaolinite compared to that of ZnO NPs.[31] Gupta et al. has reported the reduction of toxicity of ZnO NPs after the formation of heteroagglomeration with montmorillonite.[32] However, to the best of our knowledge, there is a dearth of contemporaneous and simultaneous investigations on antibacterial potential and toxicity of ZnO/clay nanostructures. Bentonite, a clay mineral mostly consisting of montmorillonite, has been used for many dermatologic formulas and in granular form is also studied for battlefield wound dressing.[33] Therefore, it is hypothesized that the ZnO NPs impregnated Bentonite: ZB nanocomposites (ZB NCs) may not only sustain the antibacterial activity of ZnO NPs by reducing the particle agglomeration but also downregulate the nonspecific toxicity toward healthy cells.

The efficacy of this NCs should be more efficient than other NCs as ZnO nanoparticles have significant antibacterial efficacy. The suggested mode of action of zinc oxide (ZnO) involves the generation of reactive oxygen species, which increases membrane lipid peroxidation and results in membrane leakage of reducing sugars, DNA, and proteins, decreasing the cell viability. The use of bentonite clay in the current work enriches the research in several ways. In contrast to earlier research, the inclusion of clay aids in the diffusion of NPs and significantly lowers the material's toxicity, expanding its utility as a therapeutic agent in the treatment of bacterial infections.

To validate the hypothesis, we have reported the synthesis of ZB NCs by impregnation of ZnO on a Bentonite surface by precipitation technique followed by calcination at 400 °C. Structural and morphological features of the NCs are studied by various characterization techniques. The toxicity of the resultant NC system was found to be less than ZnO NPs toward HEK 293 and HCT 116 cells. Moreover, antibacterial activity of ZB NCs was investigated against MDR *E. coli* (ATCC 8739) and shown to be comparable to that of ZnO NPs. In vitro antibacterial studies also supported the above findings. Our investigation and corresponding results corroborate the proposed hypothesis, where ZB NCs can be used as a potential antibacterial agent against MDR *E. coli*.

2. MATERIALS AND METHODS

2.1. Chemicals and Reagents. Sodium chloride (NaCl), thiazolyl blue tetrazolium bromide (MTT) extrapure AR (98%), and crystal violet were purchased from SRL, Mumbai. Nutrient agar (NA), nutrient broth (NB), zinc nitrate hexahydrate (ZNH) reagent grade 98%, and ferric chloride hexahydrate (FCH) ACS reagent 97% were procured from Hi-Media, Mumbai. Sodium hydroxide (NaOH) and trisodium citrate dehydrate (TCD) were purchased from Sigma-Aldrich. Fluorescein diacetate (FDA), propidium iodide (PI), and agarose were obtained from Merck Millipore, Germany. Antibodies used in this investigation were obtained from Thermo Fisher Scientific, USA. Cell culture polystyrene plates were bought from Nest Biotechnology, USA. All the cell lines were obtained from American Type Culture Collection (ATCC, USA) for a biocompatibility study. Cytotoxicity study was investigated against human col on colorectal carcinogen (HCT 116, ATCC, CCC-24) and human embryonic kidney (HEK 293, ATCC, CRL 1573) cell lines. Cell lines were kept in Dulbecco's Modified Eagle Media (DMEM) with 10% fetal bovine serum (FBS) in a humidified incubator at 37 °C and 5% CO_2 (New Brunswick, Eppendorf, USA). DMEM, FBS, and Bentonite (Purity: 99.9%, APS: <80 nm) were purchased from HiMedia.

2.2. Materials Synthesis and Processing. ZB NCs was synthesized via precipitation technique. 2 g of Bentonite clay was added to 500 mL of deionized water (DI) in a conical flask and stirred for 1 h followed by the addition of ZNH, TCD, and FCH to the solution. Furthermore, 250 mM (250 mL) NaOH was added dropwise to the above suspension using a buret.[34] This process was done until formation of a white precipitate in the flask. The solution was kept under stirring for 3 h and then cooled to room temperature (RT) and left undisturbed for 12 h. DI water was used for washing the precipitate formed to eliminate excess NaOH and dried at 60 °C for 12 h. To obtain ZB NCs, the dried mass was calcined in a muffle furnace at 400 °C for 4 h.[35]

2.3. Material Characterization. The formation of ZB NCs were confirmed by UV−visible spectroscopy. The crystal structure and particle morphology of the ZB NCs were analyzed by X-ray diffraction (XRD) (D/Max 2005, Rigaku) and transmission electron microscopy (TEM) (JEOL-JEM2010), respectively. Surface morphology and elemental

https://doi.org/10.1021/acsomega.3c07950
ACS Omega 2024, 9, 2783−2794

analysis of the ZB NCs were carried out by scanning electron microscopy (SEM) with energy-dispersive X-ray spectroscopy (EDS) (ZEISS Supra-40). The average particle size of the composite was also evaluated by a particle size histogram. Surface functional groups of the NCs were observed using Fourier transform infrared (FTIR) spectroscopy (Shimadzu 8201PC, Japan). The surface area and pore size distribution were determined by a Quantachrome NOVA 2200 system using Brunauer−Emmett−Teller (BET) and Barrett−Joyner−Halenda (BJH) techniques, respectively. Raman spectroscopy was used to study the chemical structure and crystallinity of the synthesized material.

2.4. Cytotoxicity of Materials. Toxic impact of Bentonite, ZnO NPs, and ZB NCs were checked against HCT 116 (malignant) and HEK 293 (nonmalignant) cell lines. To check the viability, all the above cells (5×10^4) were plated in a 24-well cell culture plate and incubated until it attained ∼80% confluency. The old medium was discarded with the help of aspirator. Subsequently, materials prepared in fresh DMEM with 10% FBS in different concentrations (25, 50, 75, 100, and 150 mg/mL) were added into respective wells except control, which was assigned as untreated sample. After incubation of 24 h, the MTT assay was performed.[26]

2.5. Fluorescence-Activated Cell Sorting. Fluorescence-activated cell sorting (FACS) was performed to check the occurrence of viable and nonviable cells after treatment with Bentonite, ZnO NPs, and ZB NCs. Uptake of PI by cells was assessed using FACS in accordance with the previously reported protocol.[36] HCT 116 and HEK 293 cell lines (5×10^4 cells/well) were seeded in a 24-well cell culture plate and placed in an incubator for 24 h at 37 °C with 5% CO_2. Following the incubation, the cells were supplemented with 100 mg/mL of materials (Bentonite, ZnO, and ZB NCs). The cells were then resuspended in 1× PBS (pH 7.4) before being incubated at 37 °C for 15 min with PI at a concentration of 50 mg/mL in each well. The samples were examined using a FACS Calibur flow cytometer and CELL-Quest software (Becton-Dickinson, BD Biosciences, Franklin Lakes, NJ). A total of 10,000 cells were analyzed in each sample.

2.6. Assessment of Nuclear Morphology. Genotoxicity of all the synthesized nanomaterials were checked against HCT 116 and HEK 293 cell lines using DAPI stain ≥98% (HPLC). For this study, 80% of the confluent cells were incubated for 24 h at 37 °C with ZB NCs at a concentration of 100 mg/mL. DAPI (10 μg/mL) in 1× PBS was added to each well, and the wells were incubated for 15 min in the dark at RT. Images were captured using a fluorescence microscope.[25]

2.7. DNA Degradation Assay. The cell lines used in the study were grown to 80% confluency before being treated with 100 mg/mL materials (Bentonite, Zinc oxide NPs, and ZB NCs) for 24 h. DNA was isolated from treated and control cells as per protocol.[37] Tris EDTA buffer (for molecular biology, pH 7.4) was used to dissolve the extracted DNA pellets. DNA samples (5 μL) were differentiated on a 0.8% agarose gel followed by staining with ethidium bromide (1% solution in water) for electrophoresis. A gel documentation system was used to capture the image (Gel DocTM EZ Imager, Bio-Rad).

2.8. Expressions of Cancer Markers. 100 mg/mL of Bentonite, ZnO NPs, and ZB NCs each were added to HCT 116 and HEK 293 cell lines. These samples were considered treated specimens. Control samples were not treated with the synthesized nanomaterials. The protein was obtained using radio immunoprecipitation assay buffer (Sigma-Aldrich) for use with mammalian cell and tissue extracts and DMSO solution, and the concentration was determined by Bradford assay. Protein (2 μg) samples were separated using electrophoresis on a sodium dodecyl sulfate polyacrylamide gel (10% SDSPAGE). The bands were transferred on a polyvinylidene difluoride (PVDF) membrane and incubated with a primary antibody (Cyt *c*, p16, p53, and GAPDH). PVDF membranes with the appropriate primary antibody were treated with a secondary antibody conjugated to horseradish peroxidase (HRP) and complex immune compounds. Furthermore, these were demonstrated using an enhanced chemiluminescent substrate for HRP. The assay was carried out as per manufacturer instruction (Thermo Fisher Scientific, USA).[38]

2.9. Antibacterial and Antibiofilm Activity. MDR *E. coli* was used as a test pathogen to estimate the antibacterial efficacy of ZB NCs. At first, the MDR *E. coli* culture was grown overnight in NB. Furthermore, the grown bacterial cells (1×10^6 CFU/mL) were treated with different concentrations of the synthesized NCs (10, 30, and 50 mg/mL) for 24 h at 37 °C. Cells without any treatment with NCs was taken as control. Following incubation, both the treated and control samples were plated on NA. The colonies formed were counted to estimate the CFU (colony forming unit) of bacteria. Furthermore, to evaluate the antibiofilm efficacy, *E. coli* cells were incubated with different concentration of ZB NCs (10, 30, and 50 mg/mL) for 24 h. Control samples did not contain any treatment with NCs. Following incubation, the biomass of treated and control samples were stained with Crystal Violet. Biomass survival in treated cells was calculated using the below formula[25]

$$\%\ \text{biomass} = \frac{\text{treatment abs}^{590\text{nm}} - \text{blank abs}^{590\text{nm}}}{\text{control abs}^{590\text{nm}} - \text{blank abs}^{590\text{nm}}} \times 100$$

2.10. Live/Dead Assay. To determine the viability of the bacterial cells, a live/dead assay was performed. MDR *E. coli* cells (1×10^6 CFU/mL) were treated with 50 mg/mL ZB NCs and incubated at 37 °C for 12 h along with control. The staining was carried out in accordance with the manufacturer's instructions (Bacterial Viability Kit, InvitrogenTM). Images were captured at a 100 μm scale using a fluorescence microscope (Life Technologies, USA) with a green and red filter (40× objective lens).

2.11. In Vitro Antibacterial Activity. To check the antibacterial activity in vitro, HCT 116 and HEK 293 cells were seeded in a 12 well cell culture plate and incubated with 5% CO_2 for 24 h at 37 °C to attain proper confluency. MDR *E. coli* was added to the cells by multiplicity of infection 10 (MOI-10) and the cells incubated for 1 h. ZB NCs, in different concentrations (10 and 50 mg/mL), were added to the cells after infection and rested overnight.[25] The CFU/mL of each bacterium in treated and untreated cells were calculated accordingly.[25]

2.12. Statistical Assessment. One- and two-way analysis of variance (ANOVA) was performed by PRISM (GraphPad, San Diego, CA). All the tests were done three times and the results were reported as ±standard error of the mean. The variances were found to be statistically significant at $p < 0.05$. The image captions specify a statistically significant point of analysis.

https://doi.org/10.1021/acsomega.3c07950
ACS Omega 2024, 9, 2783−2794

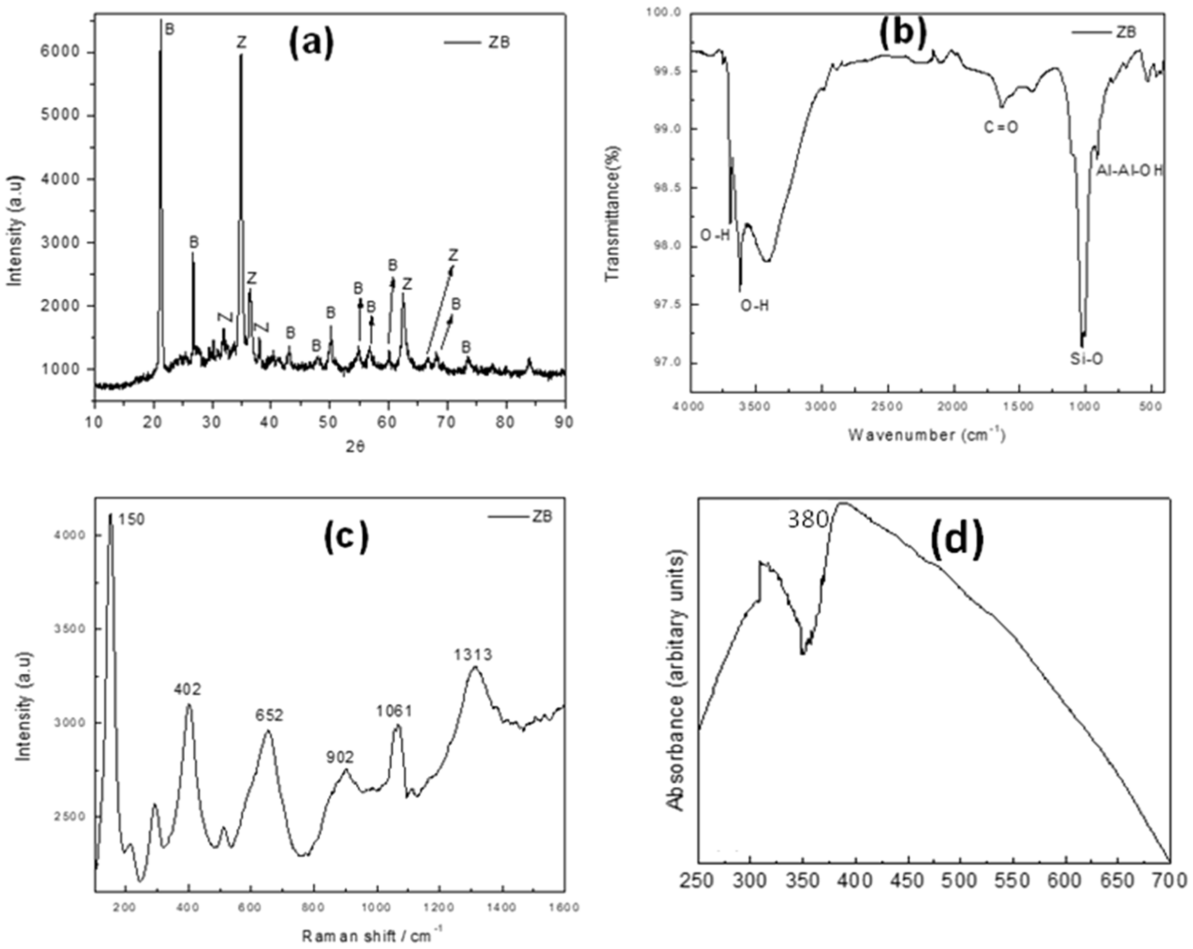

Figure 1. (a) XRD pattern of the BZ NCs. B and Z represent Bentonite and ZnO, respectively, (b) FTIR spectra of BZ NCs, (c) Raman spectra of BZ NCs, and (d) UV−visible spectroscopy of BZ NCs.

3. RESULTS AND DISCUSSION

3.1. Characterization of the Synthesized NCs. Structural and morphological features of the NCs are known to have a significant impact on their performance. Therefore, XRD analysis was performed to determine the crystal structure and phase of the ZnO NPs impregnated Bentonite: ZB NCs, and the results are shown in Figure 1a. The peaks at 2θ = 34.89, 36.63, 66.93, and 62.72° correspond to (002), (101), (103), and (110) planes of ZnO, respectively.[39,40] These could be assigned to the Wurtzite structure of ZnO. Furthermore, notable peaks at 2θ = 21.23, 27.01, and 55.02° represent the (110), (210), and (144) planes of Bentonite. These XRD patterns correlate well with the typical JCPDS file no. 01-088-0891.[41] Usually, the increasing of the intensity of XRD is accompanied by the decreasing of the full width half-maximum. Our data suggest that the order of materials through the preferred orientation of (002) is more than that of other planes. This indicates the formation of more hexagonal phase with preferred growth along the (002) plane than that of uniform growth to produce a cubic structure.[42] Interestingly, the montmorillonite making up bentonite is an aluminum phyllosilicate mineral whose crystal structure is described as low-charge tetrahedra−octahedra−tetrahedra (TOT layer unit). This means that a crystal of montmorillonite consists of layers, each of which is made up of two T sheets bonded to either side of an O sheet.[43] This unique structure of the bentonite may have provided the base for the growth of ZnO along the (002) plane, leading to a hexagonal geometry. As the reviewer has suggested, this unique feature could have reduced the leaching of free zinc ions to the biological system and hence could have shown less toxicity toward mammalian cells.[44]

Other small minute peaks can be assigned to the impurities present in the clay. However, a significant peak at 2θ = 36.9 is observed, which is similar to the major peak of ZnO equivalents to the (101) plane having a hexagonal close pack structure. Through Scherrer's equation, the mean crystallite diameter of ZB NCs is calculated to be 24 nm.

FTIR analysis was used to identify the functional groups present on the surfaces of the synthesized ZB NCs. FTIR measurements in the 500−4000 cm^{-1} range were performed to explore the surface properties of ZB NCs. Peaks at 1637 and 906 cm^{-1} in Figure 1b confirm the presence of bending vibrations of Si−O and Al−O−Al−OH active functional groups of Bentonite clay.[45] Besides, a medium intensity peak at 1027 cm^{-1} is relatively attributed to the C═O group of the carboxylic acid functional group. Furthermore, structural stretching vibrational peaks emerging at 3700−3400 cm^{-1} confirm the presence of the O−H stretching bond in ZB NCs.[46−48] Particularly, the peak at 3620 cm^{-1} derives from Al_2OH stretching.[49] A broad peak at 3496 cm^{-1} corresponds to the −OH stretching of the hydroxyl group that got deposited on the surface of ZB NCs.[50]

https://doi.org/10.1021/acsomega.3c07950
ACS Omega 2024, 9, 2783−2794

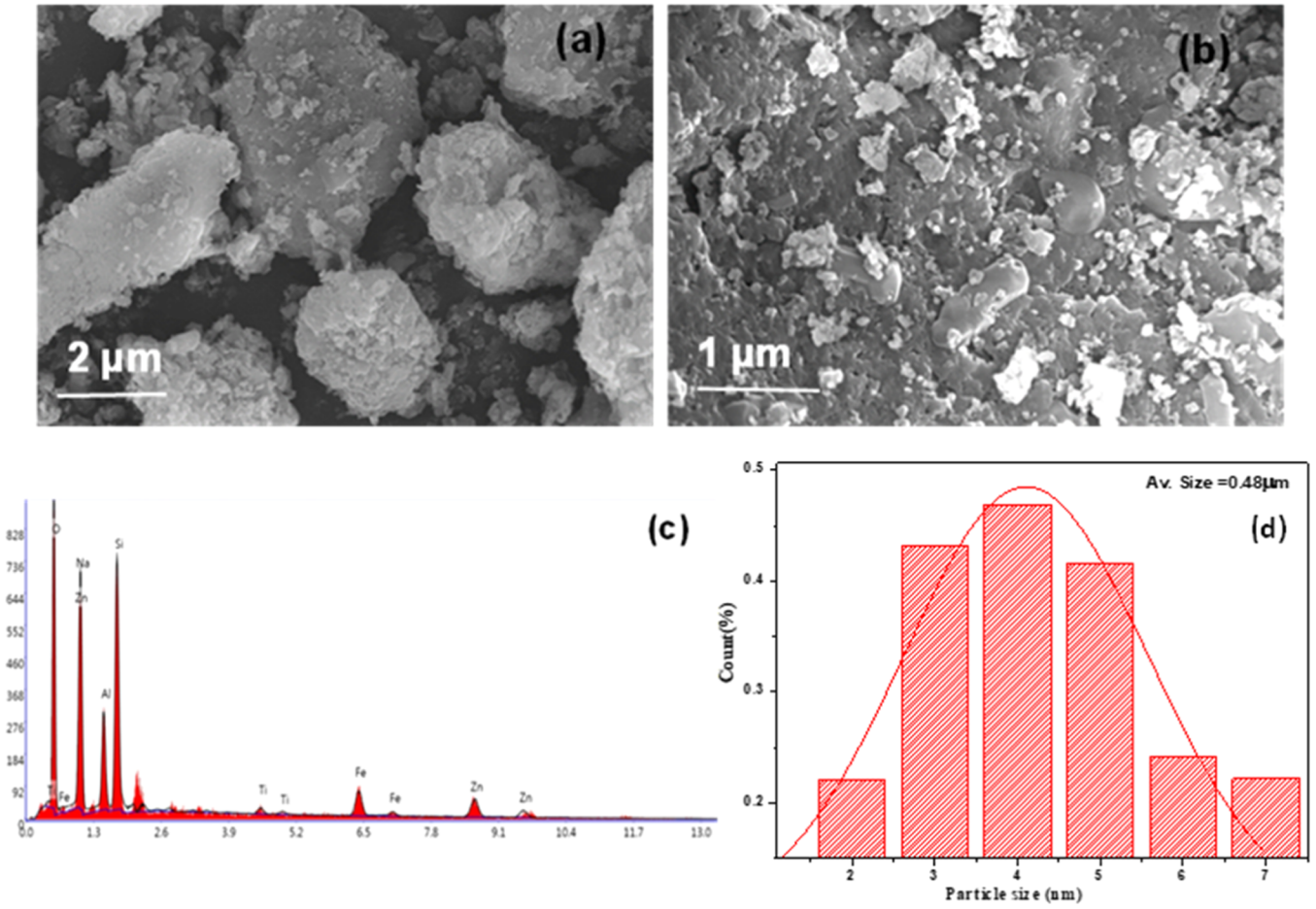

Figure 2. (a,b) SEM images of ZB NCs and (c) SEM-EDS spectra of respective material. (d) Particle size histogram of the NCs.

The Raman analysis of synthesized ZB NCs is shown in Figure 1c. For synthesized ZB, Figure 1c shows six strong peaks at 150, 402, 652, 902, 1061, and 1313 cm^{-1}. The prominent peaks at 150 cm^{1} and 402 cm^{1} are typical of ZnO in the composite.[51] They correspond to phonon frequencies *E*2low and *E*2high, respectively.[52] The process *E*2high *E*2low[52] is linked to the peak at 330. The stretching and wagging vibrations of the oxygen atom in the silica framework are seen in the Raman spectra of Bentonite at 448 and 615 cm^{-1}, respectively. The silica framework (−Si−O−Si−) is responsible for the peak at 899 cm^{-1}.[52] In conclusion, the ZB NCs employed in this work efficiently correspond to ZnO NPs and Bentonite clay according to the examination of this spectrum. Using an Agilent Cary 100 UV−Vis spectrophotometer, the absorbance spectra of ZB NCs powder in aqueous dispersion were recorded. The ZB NCs results are shown in Figure 1d. The zinc oxide may be responsible for the absorption peak at 380 nm.

The surface morphology of NCs may have a significant impact on their biocompatibility. Surface morphology of ZB NCs and its EDS spectra has been displayed in Figure 2a−c and the average particle size was calculated 0.45 μm d. It is observed that due to slight agglomeration, particles are found to be in little elongated shape with a dimension of 1 μm. Previous studies yielded similar results. Furthermore, the resulting EDS spectra of ZB NCs is shown in Figure 2c in order to survey different elemental compositions. Presence of the elements of O (47.70%), Na (22.46%), Al (6.98%), Si (15.77%), Ti (0.42%), Fe (2.89%), and Zn (3.77%) in ZB NCs validate the successful incorporation of ZnO in Bentonite.

For understanding the morphological and structural properties of the synthesized ZB NCs, TEM was performed.[52] From Figure 3a, it is evident that a thin shell of ZnO is deposited on

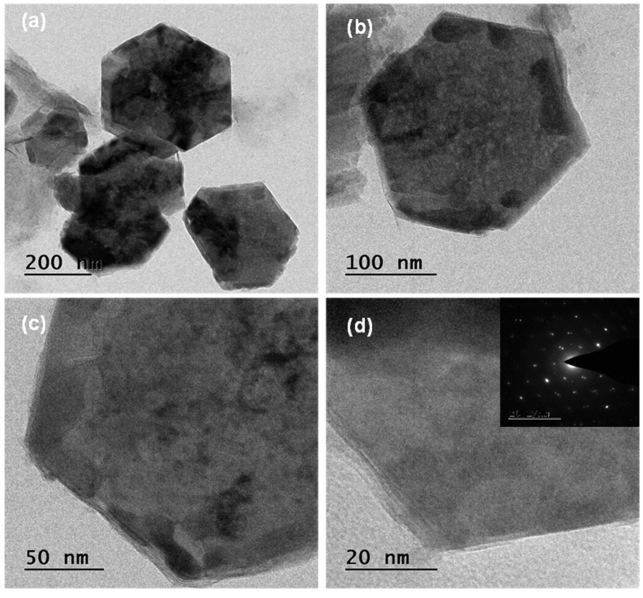

Figure 3. (a−d) TEM images of ZB NCs.

https://doi.org/10.1021/acsomega.3c07950
ACS Omega 2024, 9, 2783−2794

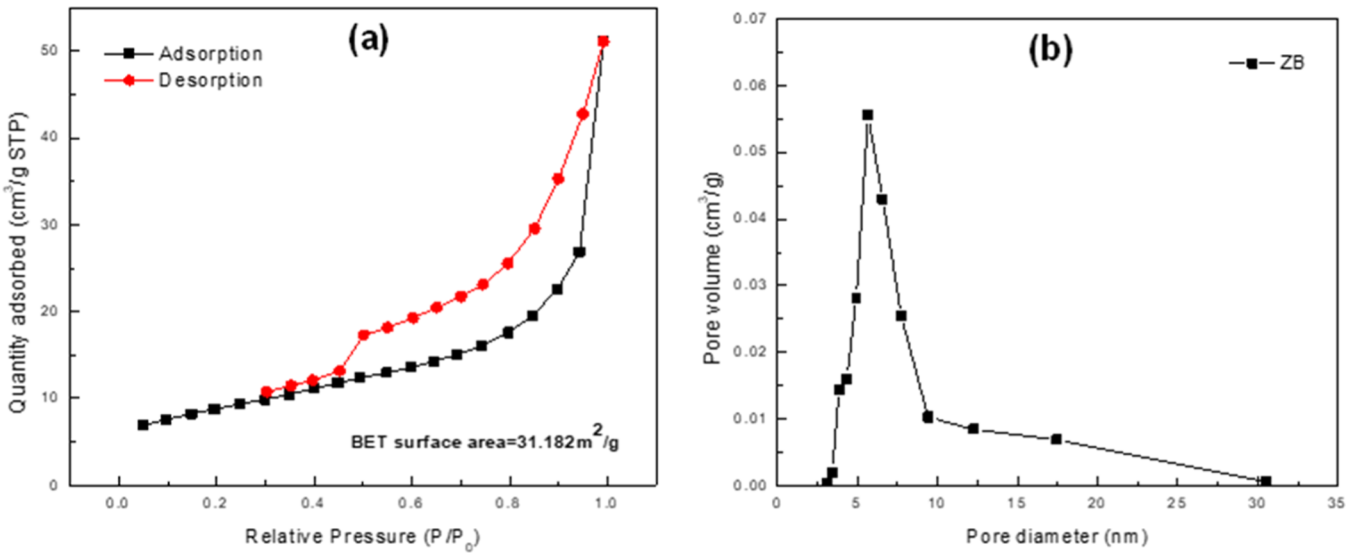

Figure 4. (a) N2 adsorption−desorption (BET) isotherm, and (b) BJH pore size distribution curve of ZB NCs.

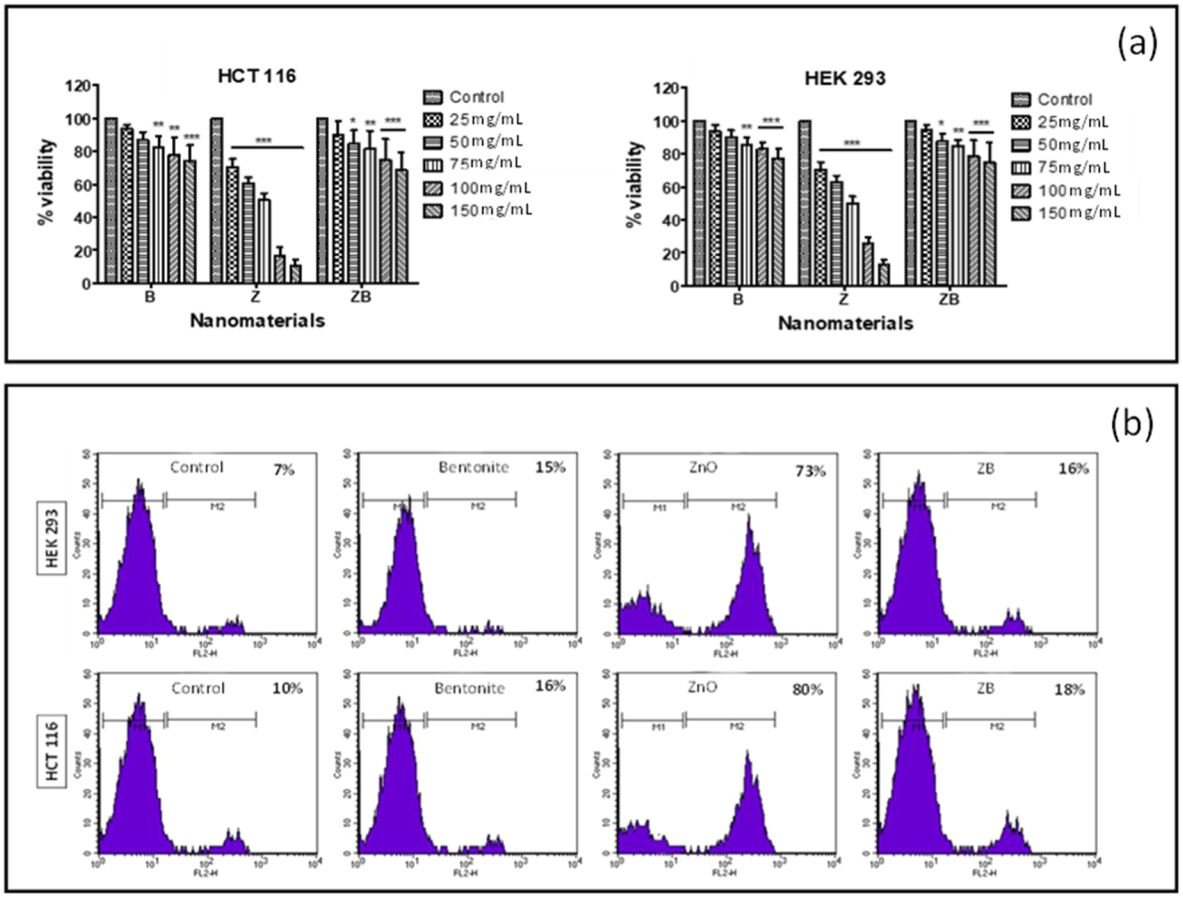

	Control	Bentonite	ZnO	ZB
HEK293	7	15	73	16
HCT116	10	16	80	18

Figure 5. Cytotoxicity of the ZB NCs was evaluated using HEK293 and HCT116 cell lines by the MTT assay (a) and FACS (b).

https://doi.org/10.1021/acsomega.3c07950
ACS Omega 2024, 9, 2783−2794

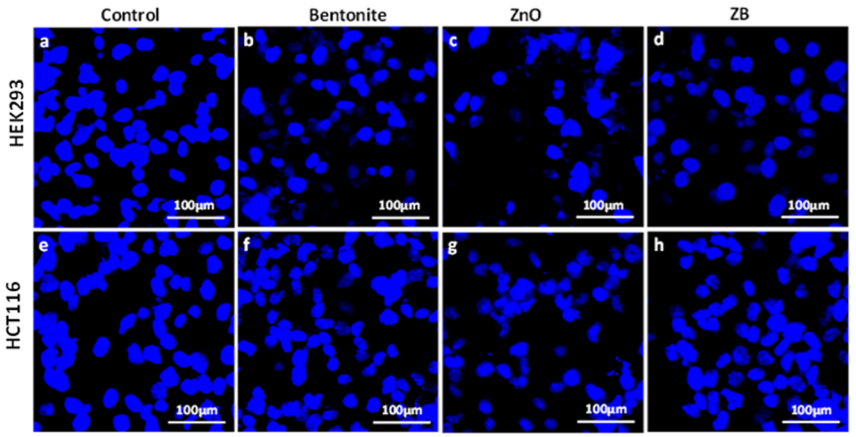

Figure 6. DAPI of HEK293 and HCT116 cells after treatment with 100 mg/mL of nanomaterials.

the surface of the Bentonite NPs. The size of ZnO NPs is reported to be in 5−10 nm range. TEM examination (Figure 3b−d) yielded more realistic evidence, such as multiple exposed crystal faces from different angles, where ZB NCs looked to be in 20−50 nm range. Selected area electron diffraction pattern implies that a polycrystalline ZB NCs system has formed. ZnO has a distinct contour that is followed by a few brighter and more conspicuous spots arranged around the ring framework, acknowledging the fact that massive crystallites are present in the nm range but in an informal manner. Furthermore, a modest increase in NC size might be due to particle agglomeration during sample preparation for TEM imaging.

Figure 4a depicts BET analyses, while b shows BJH analyses for the surface area and pore size distribution of ZB NCs. The nitrogen adsorption/desorption isotherm of ZB NCs can be allocated to the Type-II isotherm hysteresis loop group according to the IUPAC ranking. With a relative pressure (P/P_0) range of 0.407−0.985, the BET surface area of ZB NCs was determined to be 31.182 m^2/g, respectively. BJH plot distribution of ZB NCs may have a main pore size distribution peak concentrated at 5.65 nm, as inferred from Figure 4b.

3.2. Viability Assessment of Cells after Treatment with Nanomaterials. Biocompatibility testing is essential for proposing biomedical applications for any type of NCs.[53] Hence, a comparative toxicity of Bentonite, ZnO, and ZB NCs was investigated against malignant and nonmalignant cells by the MTT assay. Results shown in Figure 5a for HCT 116 cells advocate that Bentonite and ZB NCs have shown better biocompatibility toward HCT 116 cells as compared to ZnO. After the treatment with low concentrations (25, 50, and 75 mg/mL) of Bentonite, % viability of HCT 116 is detected between 85 and 90%, whereas little decrease in the growth of HCT 116 cells has been observed with 100 and 150 mg/mL (78 and 75% respectively) of the material. Similarly, for the HEK 293 cell line, from the data, it can be observed that for 25−100 mg/mL of Bentonite, viability is found to be above 85% but partial decrease in % viability (∼80%) is detected with 150 mg/mL of the clay material. The results suggest, high biocompatibility of Bentonite toward the cells used in the study. Previous studies have shown minimal toxicity of clay particles toward biological cells.[54] Contrary to the above data, in the presence of ZnO NPs at concentrations of 25, 50, 75, 100, and 150 mg/mL, the toxicity is observed to be higher for HCT 116 cell since growth has considerably reduced with the % viability being 70, 60, 50, 20 and 10%, respectively. ZnO at lower concentrations (25 and 50 mg/mL) have possessed toxicity toward HEK 293 and % viability is around 65% as compared to untreated cells. With 75, 100, and 150 mg/mL of ZnO, % viability of HEK 293 cells is observed to be nearly 50, 20, and 10%, respectively, which suggests that higher concentrations of ZnO reduced the growth of HEK 293 cells. Our results for the toxic behavior of ZnO is similar to earlier reports.[32,55] The toxicity of ZnO is mainly attributed to the generation of reactive oxygen species leading to oxidative stress and cellular membrane damage.[56] In order to reduce the toxic impact of the ZnO NPs, ZB NCs have been synthesized as the clay material incorporated with the NCs are biocompatible in nature, and their invitro toxicity has also been investigated. The treatment of different concentrations of ZB NCs (25, 50, 75, 100, and 150 mg/mL) on HCT 116 cells has shown around 75% cell survivability. Growth of HEK 293 has been observed to be above 80% after the treatment with 25, 50, 75, and 100 mg/mL ZB NCs. Nearly 75% viability of HEK 293 cells is found after treatment with 150 mg/mL ZB NCs. In the case of ZB NCs, the average % viability of the cell line is found to be ∼80%. Results obtained from above study strongly suggest that the formation of ZB NCs has down-regulated the toxicity of ZnO NPs toward mammalian cells.

3.3. Flow Cytometry Analysis of Cells. FACS is a technique for observing a specific cell population in order to gain a better knowledge of its morphological properties.[57] The uptake of PI by cells after treatment with 100 mg/mL nanomaterials has been analyzed by FACS and obtained results are shown in Figure 5b. A slight uptake of PI has been detected in all the untreated cells, and is observed to be 7 and 10% in HEK 293 and HCT 116 cells, respectively. As compared to untreated cells, a very low increment of PI uptake in Bentonite-treated HEK 293 and HCT 116 cells is detected, which is found to be 15 and 16% correspondingly. However, after treatment with ZnO, an excessive increase in the PI uptake (73 and 80%) has been observed in the HEK 293 and HCT 116 cell line, which confirms that ZnO has shown greater toxicity. Conversely, ZB NCs have been found to be less toxic toward both the cell lines and hence only 16 and 18% uptake of PI is detected. Acquired results from the above study indicate that ZB NCs and Bentonite are more biocompatible than ZnO, which is also reinforced from the MTT data.[58]

3.4. Evaluation of Genotoxicity of Nanomaterials. For confirming alteration in the nuclear morphology of the cell

https://doi.org/10.1021/acsomega.3c07950
ACS Omega 2024, 9, 2783−2794

lines following treatment with the synthesized nanomaterials, genotoxicity was investigated by means of DAPI.[59] To accomplish this study, HCT 116 and HEK 293 cells were treated with 100 mg/mL of Bentonite, ZnO, and ZB NCs for 24 h. Obtained results from fluorescence microscopy are illustrated in Figure 6. It can be seen from Figure 6a,e that both HEK 293 and HCT 116 untreated (control) cells retained their nuclear morphology. After treatment with Bentonite, considerable changes in the nuclear morphology for both cells have not been observed (Figure 6b,f). This could be due to the biocompatible property of the material toward the cell lines used in the present study. Conversely, reduction in the populations of both cell lines along with alteration and slight damage in the nuclear morphology have been found after exposure to ZnO NPs (Figure 6c,g). The altered nuclear morphology supports the cytotoxicity data, thereby indicating the toxic impact of ZnO NPs against the cell lines. However, HEK 293 and HCT 116 cells treated with ZB NCs did not show any remarkable change in nuclear morphology, as seen in Figure 6d,h. The resultant NCs system has retained the nuclear structure of both cell line. Our data corroborate with earlier findings, where toxic impact of ZnO NPs have been reduced by coating ZnO with a more biocompatible material.[25]

3.5. DNA Degradation Assay. Sometimes, nanomaterials are known to induce cell membrane damage due to the degradation of the genetic material (DNA) of the cell.[60] To validate the above, the effect of as synthesized nanomaterials on DNA of the cell has been analyzed, and obtained results are shown in Figure 7a. A thick band for HEK 293 DNA is observed for untreated (control) and Bentonite-treated sample. However, the DNA band of the above cell line has partially decreased after treatment with ZB NCs. HEK 293 when treated with ZnO NPs have shown degradation of DNA since a very thin band is identified in the gel image as compared to the ZB NC-treated sample. Similarly, DNA band of HCT 116 is found to be thick and similar to control after treatment with Bentonite. ZB NCs did not show too much effect on HCT 116 DNA since the band appeared to be thick and intense, indicating lesser cytotoxic effect of the material against the cell line. A decrease in the thickness of DNA band is spotted in ZnO-treated HCT 116 cells which appeared to be faint compared to other treated samples. From the above results, it can be concluded that changes in the DNA band is not observed after the treatment with Bentonite and ZB NCs but degradation of DNA can be seen in the ZnO-treated sample for both the cell lines.[55,61] This could be due to membrane damage to cells by ZnO NPs.

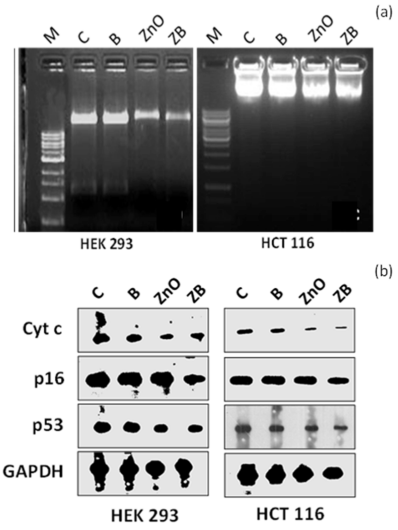

Figure 7. Effect of nanomaterials on the DNA of HEK 293 and HCT116 cells (a) and further Western blotting has been done to investigate the expression of some cancer genetic markers (b).

3.6. Expression of Cancer Markers. A cancer marker is a protein that cells produce in response to external stimuli. The presence of these indicators reveal whether a particular compound is carcinogenic or noncarcinogenic in nature.[62] The expression of some important cancer genetic markers in HEK 293 and HCT 116 cells was investigated through Western blotting after treatment with 100 mg/mL of Bentonite, ZnO, and ZB NCs. The expression of Cyt *c*, p16, and p53 were compared with GAPDH, and the obtained result is shown in Figure 7b. It can be noticed that the expression of cytochrome *c* (Cyt *c*) was maintained in untreated (control), Bentonite, and ZB NC treated cells, whereas partial down-regulation of Cyt *c* was found in ZnO treated cells. Interestingly, there was a slight downregulation in the appearance of p16 and p53 bands after treatment with ZnO NPs as compared to control. There was a slight down-regulation of p16 and p53 bands following treatment with ZB NCs. From the above data, it can be inferred that the synthesized NCs has negligible carcinogenic effect on both the cell lines. Our results align with earlier studies where coating of oxide NPs with a lesser toxic material can reduce the carcinogenic impact on cell lines.[62]

3.7. Evaluation of Antibacterial and Antibiofilm Activity. ZnO-based NCs have been widely employed as antibacterial agents due to their remarkable antibacterial activity against a broad spectrum of microorganisms.[63] However, their increased toxicity toward different cell lines have prevented their use in clinical environments.[64−67] Interestingly, NC systems with ZnO NPs have shown potential antibacterial activity with reduced toxicity toward cell lines.[31,32,68,69] Hence, in the present study, the antibacterial efficacy of the ZB NCs was evaluated against MDR *E. coli*. Different concentrations of ZB NCs were found to be effective in limiting the development of the test pathogen, as shown in (Figure 8a). When treated with the 50 mg/mL ZB NCs, there was a considerable reduction in bacterial growth (up to 5 logs) as compared to the control after 24 h of incubation. For persistent bacterial infections, biofilms play a very important role. Biofilms can be a problematic situation since bacterial biofilms are resistant to antibiotic treatments.[70−73] In this regard, in the present study, the antibiofilm activity of as synthesized ZB NCs was also evaluated against the test pathogen MDR *E. coli*. It has been observed that % biomass present in the biofilm reduced remarkably with the increase in the concentration of ZB NCs. The % biomass of MDR *E. coli* got down to almost 50% (Figure 8b) when treated with 50 mg/mL of the composite material. From the result, it can be suggested that ZB NCs have good biofilm destructive efficiency. Hence the synthesized NCs system can be scaled up and used as a potential antibacterial agent while being biocompatible in nature.

3.8. Validation of Bacterial Cell Viability by Live/Dead Staining. Fluorescence microscopy is used to observe the cellular morphology of individual cells. In this context, the test pathogen was stained with SYTO9 and PI to determine their

https://doi.org/10.1021/acsomega.3c07950
ACS Omega 2024, 9, 2783−2794

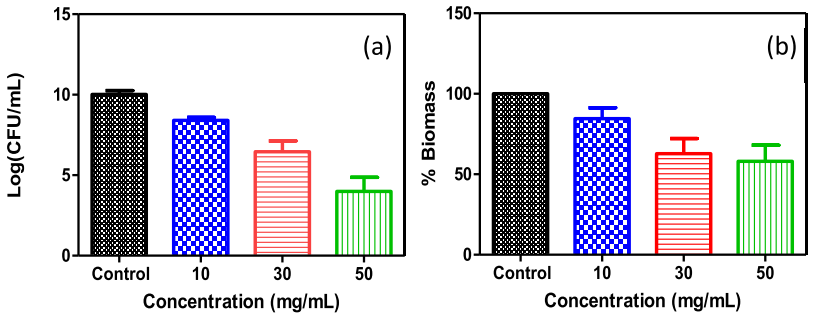

Figure 8. (a,b) Antibacterial and antibiofilm activity of ZB NCs was evaluated against MDR *E. coli*. Experiments were done in triplicate, and represented data are the standard error mean (±) of triplicate samples.

viability with and without treatment with ZB NCs. In the untreated sample, there were no dead cells, as shown in Figure 9a. In treated samples, however, more than 80% of the cells

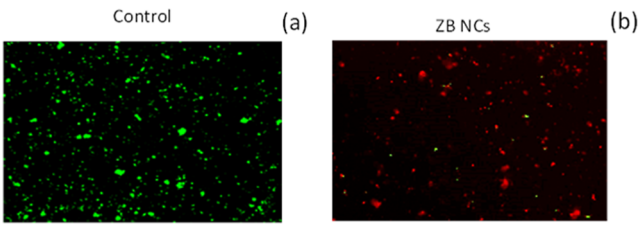

Figure 9. Qualitative viability of MDR *E. coli* was done through live/dead assay and observed under a fluorescence microscope. Untreated cells were used as the control (a) and for treatment, cells were incubated with 50 mg/mL of ZB NCs for 24 h at 37 °C (b).

were dead (Figure 9b). This set of results indicates that bacterial cell growth is inhibited in the presence of 50 mg/mL ZB NCs. The microscopy results further support the antibacterial and antibiofilm data obtained for the synthesized ZB NCs.

3.9. In Vitro Antibacterial Activity of ZB NCs. To test the antibacterial effectiveness of ZB NCs in vitro, MDR *E. coli* was inoculated into two cell lines (HEK293 and HCT 116) and then treated with the aforesaid material. Both cell lines showed a slight decrease in bacterial load after treatment with 10 mg/mL NCs, as shown in Figure 10a,b. Bacterial growth was reduced by three logs when treated with 50 mg/mL of the synthesized material. From the above findings, it may be inferred that ZB NCs promote intracellular killing of the bacteria significantly under in vitro condition.s

4. CONCLUSIONS

In summary, 50 mg/mL ZnO NPs impregnated Bentonite: ZB NCs were synthesized by a precipitation technique. The biocompatibility of the synthesized ZB NCs is found to be higher for the HCT 116 (80%) and HEK 293 (85%) cell lines as compared with ZnO NPs. The study of cells using flow cytometry and fluorescence microscopy provided additional evidence in favor of this. When treated with bentonite and ZB NCs, the shape and thickness of the DNA band did not significantly change, indicating minimal damage to the genomic DNA. ZB NCs have successfully shown that it can inhibit the growth of the MDR *E. coli* strain. A 5 log reduction in the bacterial population was seen in the presence of 50 mg/mL ZB NCs, indicating its antibacterial activity. Additionally, HEK293 and HCT 116 cell lines were used to test the in vitro antibacterial activity of ZB NCs. Our results endorse the hypothesis that the formation of the ZnO NC system may not only retain the antibacterial properties of the parent structure (i.e., ZnO) but also downregulate the nonspecific toxicity toward normal cells.

AUTHOR INFORMATION

Corresponding Authors

Gausal A. Khan − *Department of Clinical Nutrition, College of Applied Medical Sciences, King Faisal University, Al Hofuf, Al Ahsa 31982, KSA*; Email: gausalk@gmail.com

Byong-Hun Jeon − *Department of Earth Resources & Environmental Engineering, Hanyang University, Seoul 04763, Republic of Korea*; orcid.org/0000-0002-5478-765X; Email: bhjeon@hanyang.ac.kr

Amrita Mishra − *School of Biotechnology, Kalinga Institute of Industrial Technology, Bhubaneswar 751024, India*; Email: amrita.mishra@kiitbiotech.ac.in

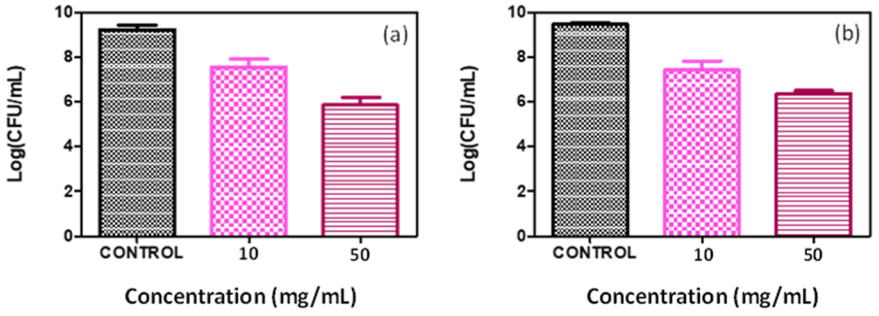

Figure 10. In vitro antibacterial activity was evaluated against MDR *E. coli* using HEK293 (a) and HCT 116 (b).

https://doi.org/10.1021/acsomega.3c07950
ACS Omega 2024, 9, 2783−2794

Authors

Susanta Kumar Behera − *School of Biotechnology, Kalinga Institute of Industrial Technology, Bhubaneswar 751024, India; IMGENEX India Pvt. Ltd., Bhubaneswar 751024, India*

Swati Sucharita Singh − *School of Biotechnology, Kalinga Institute of Industrial Technology, Bhubaneswar 751024, India*

Bhumika Jena − *School of Biotechnology, Kalinga Institute of Industrial Technology, Bhubaneswar 751024, India*

Kali Sashank − *School of Chemical Technology, Kalinga Institute of Industrial Technology, Bhubaneswar 751024, India*

Srinivas Patnaik − *School of Biotechnology, Kalinga Institute of Industrial Technology, Bhubaneswar 751024, India*

Ramesh Kumar − *Department of Earth Resources & Environmental Engineering, Hanyang University, Seoul 04763, Republic of Korea*

Sankha Chakrabortty − *School of Biotechnology, Kalinga Institute of Industrial Technology, Bhubaneswar 751024, India; School of Chemical Technology, Kalinga Institute of Industrial Technology, Bhubaneswar 751024, India;* orcid.org/0000-0001-7719-8586

Suraj K. Tripathy − *School of Biotechnology, Kalinga Institute of Industrial Technology, Bhubaneswar 751024, India; School of Chemical Technology, Kalinga Institute of Industrial Technology, Bhubaneswar 751024, India*

Complete contact information is available at: https://pubs.acs.org/10.1021/acsomega.3c07950

Notes

The authors declare no competing financial interest.

■ ACKNOWLEDGMENTS

This work was supported by the National Research Foundation of Korea (NRF) grant funded by the Korea government (MSIT) (no. RS-2023-00219983). One of the authors (R. Kumar) acknowledges the financial support through the Creative and Challenging Research Program [grant no. 2021R1I1A1A01060846] of the National Research Foundation (NRF) of the Republic of Korea.

■ REFERENCES

(1) Kolahalam, L. A.; Kasi Viswanath, I. V.; Diwakar, B. S.; Govindh, B.; Reddy, V.; Murthy, Y. L. N. Review on Nanomaterials: Synthesis and Applications. *Mater. Today Proc.* **2019**, *18*, 2182−2190.

(2) Hutchison, J. E. The Road to Sustainable Nanotechnology: Challenges, Progress and Opportunities. *ACS Sustain. Chem. Eng.* **2016**, *4* (11), 5907−5914.

(3) Theerthagiri, J.; Salla, S.; Senthil, R. A.; Nithyadharseni, P.; Madankumar, A.; Arunachalam, P.; Maiyalagan, T.; Kim, H. S. A Review on ZnO Nanostructured Materials: Energy, Environmental and Biological Applications. *Nanotechnology* **2019**, *30* (39), 392001.

(4) Noman, M. T.; Amor, N.; Petru, M. Synthesis and Applications of ZnO Nanostructures (ZONSs): A Review. *Crit. Rev. Solid State Mater. Sci.* **2022**, *47*, 99−141.

(5) Moreno-Camacho, C. A.; Montoya-Torres, J. R.; Jaegler, A.; Gondran, N. Sustainability Metrics for Real Case Applications of the Supply Chain Network Design Problem: A Systematic Literature Review. *J. Cleaner Prod.* **2019**, *231*, 600−618.

(6) Ghanbari Shohany, B.; Khorsand Zak, A. Doped ZnO Nanostructures with Selected Elements - Structural, Morphology and Optical Properties: A Review. *Ceram. Int.* **2020**, *46* (5), 5507−5520.

(7) Li, A.; Sun, H. X.; Tan, D. Z.; Fan, W. J.; Wen, S. H.; Qing, X. J.; Li, G. X.; Li, S. Y.; Deng, W. Q. Superhydrophobic Conjugated Microporous Polymers for Separation and Adsorption. *Energy Environ. Sci.* **2011**, *4* (6), 2062−2065.

(8) Fisher, R. A.; Gollan, B.; Helaine, S. Persistent Bacterial Infections and Persister Cells. *Nat. Rev. Microbiol.* **2017**, *15* (8), 453−464.

(9) Langford, B. J.; So, M.; Raybardhan, S.; Leung, V.; Westwood, D.; MacFadden, D. R.; Soucy, J.-P. R.; Daneman, N. Bacterial Co-Infection and Secondary Infection in Patients with COVID-19: A Living Rapid Review and Meta-Analysis. *Clin. Microbiol. Infect.* **2020**, *26* (12), 1622−1629.

(10) Gollan, B.; Grabe, G.; Michaux, C.; Helaine, S. Bacterial Persisters and Infection: Past, Present, and Progressing. *Annu. Rev. Microbiol.* **2019**, *73*, 359−385.

(11) Alavi, M.; Kowalski, R.; Capasso, R.; Coutinho, H. D. M.; De Menezes, I. R. A. Various Novel Strategies for Functionalization of Gold and Silver Nanoparticles to Hinder Drug-Resistant Bacteria and Cancer Cells. *Micro Nano Bio Asp.* **2022**, *1* (1), 38−48.

(12) Alavi, M.; Hamblin, M. R.; Kennedy, J. F. Antimicrobial Applications of Lichens: Secondary Metabolites and Green Synthesis of Silver Nanoparticles: A Review. *Nano Micro Biosyst.* **2022**, *1* (1), 15−21.

(13) Alavi, M.; Thomas, S.; Sreedharan, M. Modification of Silica Nanoparticles for Antibacterial Activities: Mechanism of Action. *Micro Nano Bio Asp.* **2022**, *1* (1), 49−58.

(14) Abebe, B.; Zereffa, E. A.; Tadesse, A.; Murthy, H. C. A. A Review on Enhancing the Antibacterial Activity of ZnO: Mechanisms and Microscopic Investigation. *Nanoscale Res. Lett.* **2020**, *15* (1), 190.

(15) Alhashash, F.; Weston, V.; Diggle, M.; McNally, A. Multidrug-Resistant Escherichia Coli Bacteremia. *Emerging Infect. Dis.* **2013**, *19* (10), 1699.

(16) Dadashi, M.; Sameni, F.; Bostanshirin, N.; Yaslianifard, S.; Khosravi-Dehaghi, N.; Nasiri, M. J.; Goudarzi, M.; Hashemi, A.; Hajikhani, B. Global Prevalence and Molecular Epidemiology of Mcr-Mediated Colistin Resistance in Escherichia Coli Clinical Isolates: A Systematic Review. *J. Global Antimicrob. Resist.* **2022**, *29*, 444−461.

(17) Zhang, S.; Abbas, M.; Rehman, M. U.; Wang, M.; Jia, R.; Chen, S.; Liu, M.; Zhu, D.; Zhao, X.; Gao, Q.; Tian, B.; Cheng, A. Updates on the Global Dissemination of Colistin-Resistant Escherichia Coli: An Emerging Threat to Public Health. *Sci. Total Environ.* **2021**, *799*, 149280.

(18) Zhang, L.; Jiang, Y.; Ding, Y.; Daskalakis, N.; Jeuken, L.; Povey, M.; O'Neill, A. J.; York, D. W. Mechanistic Investigation into Antibacterial Behaviour of Suspensions of ZnO Nanoparticles against E. Coli. *J. Nanopart. Res.* **2010**, *12* (5), 1625−1636.

(19) Kumar, A.; Pandey, A. K.; Singh, S. S.; Shanker, R.; Dhawan, A. Engineered ZnO and TiO2 Nanoparticles Induce Oxidative Stress and DNA Damage Leading to Reduced Viability of Escherichia Coli. *Free Radical Biol. Med.* **2011**, *51* (10), 1872−1881.

(20) Jiang, Y.; Zhang, L.; Wen, D.; Ding, Y. Role of Physical and Chemical Interactions in the Antibacterial Behavior of ZnO Nanoparticles against E. Coli. *Mater. Sci. Eng., C* **2016**, *69*, 1361−1366.

(21) Baek, S.; Joo, S. H.; Kumar, N.; Toborek, M. Antibacterial Effect and Toxicity Pathways of Industrial and Sunscreen ZnO Nanoparticles on Escherichia Coli. *J. Environ. Chem. Eng.* **2017**, *5* (3), 3024−3032.

(22) Hameed, A. S. H.; Karthikeyan, C.; Ahamed, A. P.; Thajuddin, N.; Alharbi, N. S.; Alharbi, S. A.; Ravi, G. In Vitro Antibacterial Activity of ZnO and Nd Doped ZnO Nanoparticles against ESBL Producing Escherichia Coli and Klebsiella Pneumoniae. *Sci. Rep.* **2016**, *6* (1), 24312.

(23) Naqvi, Q.-u.-A.; Kanwal, A.; Qaseem, S.; Naeem, M.; Ali, S. R.; Shaffique, M.; Maqbool, M. Size-Dependent Inhibition of Bacterial Growth by Chemically Engineered Spherical ZnO Nanoparticles. *J. Biol. Phys.* **2019**, *45* (2), 147−159.

(24) Keerthana, S.; Kumar, A. Potential Risks and Benefits of Zinc Oxide Nanoparticles: A Systematic Review. *Crit. Rev. Toxicol.* **2020**, *50* (1), 47−71.
(25) Khan, M. I.; Behera, S. K.; Paul, P.; Das, B.; Suar, M.; Jayabalan, R.; Fawcett, D.; Poinern, G. E. J.; Tripathy, S. K.; Mishra, A. Biogenic Au@ZnO Core-Shell Nanocomposites Kill Staphylococcus Aureus without Provoking Nuclear Damage and Cytotoxicity in Mouse Fibroblasts Cells under Hyperglycemic Condition with Enhanced Wound Healing Proficiency. *Med. Microbiol. Immunol.* **2019**, *208* (5), 609−629.
(26) Khan, M. I.; Paul, P.; Behera, S. K.; Jena, B.; Tripathy, S. K.; Stålsby Lundborg, C.; Mishra, A. To Decipher the Antibacterial Mechanism and Promotion of Wound Healing Activity by Hydrogels Embedded with Biogenic Ag@ZnO Core-Shell Nanocomposites. *Chem. Eng. J.* **2021**, *417*, 128025.
(27) Rao, K. M.; Suneetha, M.; Park, G. T.; Babu, A. G.; Han, S. S. Hemostatic, Biocompatible, and Antibacterial Non-Animal Fungal Mushroom-Based Carboxymethyl Chitosan-ZnO Nanocomposite for Wound-Healing Applications. *Int. J. Biol. Macromol.* **2020**, *155*, 71−80.
(28) Zhu, C.; Wang, H.; Mahmood, Z.; Wang, Q.; Ma, H. Biocompatibility and Biodegradability of Polyacrylate/ZnO Nanocomposite during the Activated Sludge Treatment Process. *PLoS One* **2018**, *13* (11), No. e0205990.
(29) Carretero, M. I.; Gomes, C. S. F.; Tateo, F. Clays, Drugs, and Human Health. *Dev. Clay Sci.* **2013**, *5* (C), 711−764.
(30) Williams, L. B. Natural Antibacterial Clays: Historical Uses and Modern Advances. *Clays Clay Miner.* **2019**, *67* (1), 7−24.
(31) Tokarský, J.; Mamulová Kutláková, K.; Podlipná, R.; Vaněk, T. Phytotoxicity of ZnO/Kaolinite Nanocomposite—Is Anchoring the Right Way to Lower Environmental Risk? *Environ. Sci. Pollut. Res.* **2019**, *26* (21), 22069−22081.
(32) Gupta, G. S.; Senapati, V. A.; Dhawan, A.; Shanker, R. Heteroagglomeration of Zinc Oxide Nanoparticles with Clay Mineral Modulates the Bioavailability and Toxicity of Nanoparticle in Tetrahymena Pyriformis. *J. Colloid Interface Sci.* **2017**, *495*, 9−18.
(33) Park, J.-H.; Shin, H.-J.; Kim, M. H.; Kim, J.-S.; Kang, N.; Lee, J.-Y.; Kim, K.-T.; Lee, J. I.; Kim, D.-D. Application of Montmorillonite in Bentonite as a Pharmaceutical Excipient in Drug Delivery Systems. *J. Pharm. Invest.* **2016**, *46* (4), 363−375.
(34) Misra, A. J.; Basu, A.; Behera, S. K.; Mishra, A.; Lundborg, C. S.; Tripathy, S. K. Point-of-Use Photocatalytic Device for Water Disinfection under Visible Light Using ZnO/Gypsum@alginate Beads. *J. Environ. Chem. Eng.* **2022**, *10* (3), 107520.
(35) Misra, A. J.; Das, S.; Habeeb Rahman, A. P.; Das, B.; Jayabalan, R.; Behera, S. K.; Suar, M.; Tamhankar, A. J.; Mishra, A.; Lundborg, C. S.; Tripathy, S. K. Doped ZnO Nanoparticles Impregnated on Kaolinite (Clay): A Reusable Nanocomposite for Photocatalytic Disinfection of Multidrug Resistant Enterobacter Sp. under Visible Light. *J. Colloid Interface Sci.* **2018**, *530*, 610−623.
(36) Gillissen, M. A.; Yasuda, E.; de Jong, G.; Levie, S. E.; Go, D.; Spits, H.; van Helden, P. M.; Hazenberg, M. D. The Modified FACS Calcein AM Retention Assay: A High Throughput Flow Cytometer Based Method to Measure Cytotoxicity. *J. Immunol. Methods* **2016**, *434*, 16−23.
(37) Das, S.; Misra, A. J.; Habeeb Rahman, A. P.; Das, B.; Jayabalan, R.; Tamhankar, A. J.; Mishra, A.; Lundborg, C. S.; Tripathy, S. K. Ag@SnO2@ZnO Core-Shell Nanocomposites Assisted Solar-Photocatalysis Downregulates Multidrug Resistance in Bacillus Sp.: A Catalytic Approach to Impede Antibiotic Resistance. *Appl. Catal., B* **2019**, *259*, 118065.
(38) Bryś, M.; Semczuk, A.; Wójcik, M.; Krajewska, W. M.; Jakowicki, J. A. P53 Protein Detection by the Western Blotting Technique in Normal and Neoplastic Specimens of Human Endometrium. *Cancer Lett.* **2000**, *148* (2), 197−205.
(39) Dou, P.; Tan, F.; Wang, W.; Sarreshteh, A.; Qiao, X.; Qiu, X.; Chen, J. One-Step Microwave-Assisted Synthesis of Ag/ZnO/Graphene Nanocomposites with Enhanced Photocatalytic Activity. *J. Photochem. Photobiol., A* **2015**, *302*, 17−22.
(40) Lin, L.; Han, Y.; Fuji, M.; Endo, T.; Wang, X.; Takahashi, M. Synthesis of Hexagonal ZnO Microtubes by a Simple Soft Aqueous Solution Method. *J. Ceram. Soc. Jpn.* **2008**, *116* (1350), 198−200.
(41) Hebbar, R. S.; Isloor, A. M.; Prabhu, B.; Inamuddin; Asiri, A. M.; Ismail, A. F. Removal of Metal Ions and Humic Acids through Polyetherimide Membrane with Grafted Bentonite Clay. *Sci. Rep.* **2018**, *8* (1), 4665.
(42) Özgür, D. C.; Alivov, Y. I.; Liu, C.; Teke, A.; Reshchikov, M. A.; Doğan, S.; Avrutin, V.; Cho, S.-J.; Morkoç, H. A Comprehensive Review of ZnO Materials and Devices. *J. Appl. Phys.* **2005**, *98* (4), 041301.
(43) Galdámez-Martinez, A.; Santana, G.; Güell, F.; Martínez-Alanis, P. R.; Dutt, A. Photoluminescence of ZnO Nanowires: A Review. *Nanomaterials* **2020**, *10* (5), 857.
(44) Sirelkhatim, A.; Mahmud, S.; Seeni, A.; Kaus, N. H. M.; Ann, L. C.; Bakhori, S. K. M.; Hasan, H.; Mohamad, D. Review on Zinc Oxide Nanoparticles: Antibacterial Activity and Toxicity Mechanism. *Nano-Micro Lett.* **2015**, *7* (3), 219−242.
(45) Maged, A.; Kharbish, S.; Ismael, I. S.; Bhatnagar, A. Characterization of Activated Bentonite Clay Mineral and the Mechanisms Underlying Its Sorption for Ciprofloxacin from Aqueous Solution. *Environ. Sci. Pollut. Res.* **2020**, *27* (26), 32980−32997.
(46) Chakraborty, T.; Chakraborty, A.; Shukla, M.; Chattopadhyay, T. ZnO-Bentonite Nanocomposite: An Efficient Catalyst for Discharge of Dyes, Phenol and Cr(VI) from Water. *J. Coord. Chem.* **2019**, *72* (1), 53−68.
(47) Tanpure, S.; Ghanwat, V.; Shinde, B.; Tanpure, K.; Lawande, S. The Eggshell Waste Transformed Green and Efficient Synthesis of K-Ca(OH)2 Catalyst for Room Temperature Synthesis of Chalcones. *Polycyclic Aromat. Compd.* **2022**, *42*, 1322−1340.
(48) Zaitan, H.; Bianchi, D.; Achak, O.; Chafik, T. A Comparative Study of the Adsorption and Desorption of O-Xylene onto Bentonite Clay and Alumina. *J. Hazard. Mater.* **2008**, *153* (1−2), 852−859.
(49) Tabak, A.; Yilmaz, N.; Eren, E.; Caglar, B.; Afsin, B.; Sarihan, A. Structural Analysis of Naproxen-Intercalated Bentonite (Unye). *Chem. Eng. J.* **2011**, *174* (1), 281−288.
(50) Hu, X.; Cheng, W.; Shao, Z. Novel Authigenic Gas Foaming Hydrogels for Preventing Coal Spontaneous Combustion. *e-Polymers* **2015**, *15* (5), 361−368.
(51) Leiva, E.; Tapia, C.; Rodríguez, C. Highly Efficient Removal of Cu(II) Ions from Acidic Aqueous Solution Using ZnO Nanoparticles as Nano-Adsorbents. *Water* **2021**, *13* (21), 2960.
(52) Arguello, C. A.; Rousseau, D. L.; Porto, S. P. S. First-Order Raman Effect in Wurtzite-Type Crystals. *Phys. Rev.* **1969**, *181* (3), 1351−1363.
(53) Witika, B. A.; Makoni, P. A.; Matafwali, S. K.; Chabalenge, B.; Mwila, C.; Kalungia, A. C.; Nkanga, C. I.; Bapolisi, A. M.; Walker, R. B. Biocompatibility of Biomaterials for Nanoencapsulation: Current Approaches. *Nanomaterials* **2020**, *10* (9), 1649.
(54) Bessa, M. J.; Costa, C.; Reinosa, J.; Pereira, C.; Fraga, S.; Fernández, J.; Bañares, M. A.; Teixeira, J. P. Moving into Advanced Nanomaterials. Toxicity of Rutile TiO2 Nanoparticles Immobilized in Nanokaolin Nanocomposites on HepG2 Cell Line. *Toxicol. Appl. Pharmacol.* **2017**, *316*, 114−122.
(55) Chang, Y.-N.; Zhang, M.; Xia, L.; Zhang, J.; Xing, G. The Toxic Effects and Mechanisms of CuO and ZnO Nanoparticles. *Materials* **2012**, *5* (12), 2850−2871.
(56) Guo, D.; Bi, H.; Liu, B.; Wu, Q.; Wang, D.; Cui, Y. Reactive Oxygen Species-Induced Cytotoxic Effects of Zinc Oxide Nanoparticles in Rat Retinal Ganglion Cells. *Toxicol. In Vitro* **2013**, *27* (2), 731−738.
(57) Liao, X.; Makris, M.; Luo, X. M. Fluorescence-Activated Cell Sorting for Purification of Plasmacytoid Dendritic Cells from the Mouse Bone Marrow. *J. Visualized Exp.* **2016**, *2016* (117), No. e54641.
(58) Kundu, M.; Sadhukhan, P.; Ghosh, N.; Chatterjee, S.; Manna, P.; Das, J.; Sil, P. C. PH-Responsive and Targeted Delivery of Curcumin via Phenylboronic Acid-Functionalized ZnO Nanoparticles for Breast Cancer Therapy. *J. Adv. Res.* **2019**, *18*, 161−172.

https://doi.org/10.1021/acsomega.3c07950
ACS Omega 2024, 9, 2783−2794

(59) Sohrabi, Y.; Mohammadzadeh-Aghdash, H.; Baghbani, E.; Dehghan, P.; Ezzati Nazhad Dolatabadi, J. Cytotoxicity and Genotoxicity Assessment of Ascorbyl Palmitate (AP) Food Additive. *Adv. Pharm. Bull.* **2018**, *8* (2), 341−346.
(60) Singh, N.; Manshian, B.; Jenkins, G. J. S.; Griffiths, S. M.; Williams, P. M.; Maffeis, T. G. G.; Wright, C. J.; Doak, S. H. NanoGenotoxicology: The DNA Damaging Potential of Engineered Nanomaterials. *Biomaterials* **2009**, *30* (23−24), 3891−3914.
(61) Chakraborti, S.; Chakraborty, S.; Saha, S.; Manna, A.; Banerjee, S.; Adhikary, A.; Sarwar, S.; Hazra, T. K.; Das, T.; Chakrabarti, P. PEG-Functionalized Zinc Oxide Nanoparticles Induce Apoptosis in Breast Cancer Cells through Reactive Oxygen Species-Dependent Impairment of DNA Damage Repair Enzyme NEIL2. *Free Radical Biol. Med.* **2017**, *103*, 35−47.
(62) Hanjani, N. A.; Esmaelizad, N.; Zanganeh, S.; Gharavi, A. T.; Heidarizadeh, P.; Radfar, M.; Omidi, F.; MacLoughlin, R.; Doroudian, M. Emerging Role of Exosomes as Biomarkers in Cancer Treatment and Diagnosis. *Crit. Rev. Oncol. Hematol.* **2022**, *169*, 103565.
(63) Kurniawan, F. H.; Chinavinijkul, P.; Nasongkla, N. Hydrophobic and Antibacterial Bed Sheet Using ZnO Nanoparticles: A Large-Scale Technique. *J. Drug Delivery Sci. Technol.* **2021**, *62*, 102339.
(64) Javed, R.; Zia, M.; Naz, S.; Aisida, S. O.; Ain, N.-u.; Ao, Q. Role of Capping Agents in the Application of Nanoparticles in Biomedicine and Environmental Remediation: Recent Trends and Future Prospects. *J. Nanobiotechnol.* **2020**, *18* (1), 172.
(65) Vakili-Ghartavol, R.; Momtazi-Borojeni, A. A.; Vakili-Ghartavol, Z.; Aiyelabegan, H. T.; Jaafari, M. R.; Rezayat, S. M.; Arbabi Bidgoli, S. Toxicity Assessment of Superparamagnetic Iron Oxide Nanoparticles in Different Tissues. *Artif. Cells, Nanomed., Biotechnol* **2020**, *48* (1), 443−451.
(66) Buerki-Thurnherr, T.; Xiao, L.; Diener, L.; Arslan, O.; Hirsch, C.; Maeder-Althaus, X.; Grieder, K.; Wampfler, B.; Mathur, S.; Wick, P.; Krug, H. F. In Vitro Mechanistic Study towards a Better Understanding of ZnO Nanoparticle Toxicity. *Nanotoxicology* **2013**, *7* (4), 402−416.
(67) Namvar, F.; Rahman, H. S.; Mohamad, R.; Azizi, S.; Tahir, P. M.; Chartrand, M. S.; Yeap, S. K. Cytotoxic Effects of Biosynthesized Zinc Oxide Nanoparticles on Murine Cell Lines. *J. Evidence-Based Complementary Altern. Med.* **2015**, *2015*, 1−11.
(68) Khan, M. I.; Mazumdar, A.; Pathak, S.; Paul, P.; Kumar Behera, S.; Tamhankar, A. J.; Tripathy, S. K.; Stålsby Lundborg, C.; Mishra, A. Biogenic Ag/CaO Nanocomposites Kill Staphylococcus Aureus with Reduced Toxicity towards Mammalian Cells. *Colloids Surf., B* **2020**, *189*, 110846.
(69) Salahuddin, N.; Awad, S.; Elfiky, M. Vanillin-Crosslinked Chitosan/ZnO Nanocomposites as a Drug Delivery System for 5-Fluorouracil: Study on the Release Behavior via Mesoporous ZrO2-Co3O4 Nanoparticles Modified Sensor and Antitumor Activity. *RSC Adv.* **2022**, *12* (33), 21422−21439.
(70) Ciofu, O.; Moser, C.; Jensen, P. Ø.; Høiby, N. Tolerance and Resistance of Microbial Biofilms. *Nat. Rev. Microbiol.* **2022**, *20* (10), 621−635.
(71) Li, C.; Cornel, E. J.; Du, J. Advances and Prospects of Polymeric Particles for the Treatment of Bacterial Biofilms. *ACS Appl. Polym. Mater.* **2021**, *3* (5), 2218−2232.
(72) Sharma, D.; Misba, L.; Khan, A. U. Antibiotics versus Biofilm: An Emerging Battleground in Microbial Communities. *Antimicrob. Resist. Infect. Control* **2019**, *8* (1), 76.
(73) Mah, T.-F. C.; O'Toole, G. A. Mechanisms of Biofilm Resistance to Antimicrobial Agents. *Trends Microbiol.* **2001**, *9* (1), 34−39.

https://doi.org/10.1021/acsomega.3c07950
ACS Omega 2024, 9, 2783−2794